Ethanol Electrooxidation on a Carbon-Supported Pt Catalyst: Reaction Kinetics and Product Yields

H. Wang, Z. Jusys,* and R. J. Behm

Department Surface Chemistry and Catalysis, University of Ulm, D-89069 Ulm, Germany

Received: August 1, 2004

The ethanol oxidation reaction (EOR) on a carbon-supported Pt nanoparticle catalyst was studied by cyclic voltammetry and potential-step measurements as a function of ethanol concentration and reaction temperature (23−60 °C), combining on-line mass spectrometric analysis of the reaction products and electrochemical current measurements. The effect of catalyst loading/electrode roughness was elucidated by comparison with a polycrystalline Pt electrode. Individual, absolute rates for CO_2 and acetaldehyde formation were determined via the doubly ionized carbon dioxide molecular ion at $m/z = 22$ and the CHO^+ fragment at $m/z = 29$, whereas acetic acid yields were calculated as the difference between the Faradaic current (charge) and the sum of the partial currents for oxidation to CO_2 and acetaldehyde, calculated from the calibrated mass spectrometric currents. Incomplete ethanol oxidation to acetaldehyde and acetic acid prevails over complete oxidation to CO_2 under all conditions, the dominant products being acetic acid at low (1 mM) and acetaldehyde at high (0.5 M) ethanol concentration or low catalyst loading/electrode roughness, i.e., on the smooth Pt electrode, whereas current efficiency and product yield for CO_2 formation is on the order of a few percent. The reaction orders for ethanol on Pt/Vulcan are 0.3, 0.6, and 0.9 for CO_2, acetic acid, and acetaldehyde formation and 0.6 for the total Faradaic current, respectively. These trends are discussed in terms of increasing readsorption and subsequent oxidation of volatile, desorbing reaction intermediates with increasing catalyst loading/electrode roughness, considering that acetic acid oxidation is kinetically hindered at room temperature, and a rather low rate for C−C bond breaking under these conditions. The temperature dependence in this temperature range results in an apparent activation energy for the total reaction (Faradaic current) of 32 kJ/mol. The respective values for the partial reactions for CO_2, acetic acid and acetaldehyde formation are 20, 28, and 43 kJ/mol, respectively.

1. Introduction

Direct alcohol fuel cells (DAFCs) are attracting increasing interest as a compact power sources for portable applications, mainly due to the relatively simple handling, storage, and transportation of the fuel. Though the interest is focused on the use of methanol because of its better reaction kinetics and hence better performance in a fuel cell, ethanol is of interest as the major renewable biofuel because it is less toxic than other alcohols. Hence, it is a promising liquid fuel for directly fueled DAFCs.[1−4] However, ethanol oxidation to CO_2 is associated with the cleavage of the C−C bond, which requires a higher activation energy than C−H bond breaking, at least for currently known electrocatalysts.[5] The efficiency for ethanol oxidation can be improved both by development of more active electrocatalysts and by optimization of the reaction parameters and conditions, e.g., by operating under conditions where the formation of poisoning reaction intermediates or the loss of volatile reaction intermediates (=partial oxidation products) is minimized. Verification of these goals requires a detailed mechanistic and kinetic understanding of the processes proceeding during electrocatalytic ethanol oxidation. Despite a significant number of studies on this topic,[1−4,6−12] our present knowledge is far from a molecular scale understanding of this reaction, which would include also a quantitative knowledge of kinetics of the most important elementary reaction steps contributing to the total reaction process. We have therefore started a comprehensive study of the reaction characteristics of the oxidation of ethanol and related C-2 molecules, applying both electrochemical measurements and in situ spectroscopic techniques.

The present mechanistic understanding of the ethanol oxidation reaction (EOR) can be summarized as follows: The reaction is known to proceed via a complex multistep mechanism, involving a number of adsorbed reaction intermediates and byproducts resulting from incomplete ethanol oxidation.[8] The major adsorbed intermediates were identified as adsorbed CO and C-1 and C-2 hydrocarbon residues, whereas acetaldehyde and acetic acid have been detected as the main byproducts using differential electrochemical mass spectrometry (DEMS), infrared spectroscopy, ion chromatography, and liquid chromatography.[3,10−12] Leung et al. have used infrared spectroscopy to quantitatively evaluate the formation of CO_{ad}, CO_2, acetaldehyde, and acetic acid on a Pt(111) electrode and showed that incomplete ethanol oxidation products prevail over complete oxidation to CO_2.[7] Tarnowski et al. have used ion chromatography to quantify the yields of acetic acid during ethanol oxidation on Pt(111), Pt(335), and Pt(557) electrode surfaces.[11] Wang et al. studied the relative product distribution during polymer electrolyte fuel cell operation with ethanol as the anode feed using on-line mass spectrometry.[1] They could show that under reaction conditions used in that study acetaldehyde is the main reaction product, whereas CO_2 is a minor product in the

* Corresponding author. E-mail: zenonas.jusys@chemie.uni-ulm.de.

10.1021/jp046561k CCC: $27.50
Published on Web 11/16/2004

temperature range between 150 and 190 °C and water: ethanol molar ratios between 5 and 2, without significant differences in the product selectivities on Pt−Ru and Pt-black catalysts. Using chromatographic techniques, Hitmi et al. found that at low ethanol concentrations the main product is acetic acid, whereas acetaldehyde prevails at high concentration (>0.1 M) during ethanol oxidation on polycrystalline Pt at 10 °C.[8] Aricò et al. investigated the electrochemical oxidation of ethanol in a liquid-feed solid polymer electrolyte fuel cell operating at 145 °C and 1 M ethanol and found that under these conditions the direct ethanol fuel cell has a high selectivity toward CO_2 formation (95%).[13] Fujiwara et al. studied ethanol oxidation on electrodeposited Pt and PtRu electrodes by DEMS and reported that PtRu gives a higher relative yield of CO_2 than pure Pt, even 100% for $Pt_{0.5}Ru_{0.5}$ at low temperatures (5 and 25 °C).[3] Finally, ethanol oxidation on Pt, PtRu, and PtRh electrodes and the nature of the reaction products has been investigated by several groups using DEMS.[6,9,14,15] In these studies it was not attempted, however, to quantify the distribution of reaction products on an absolute scale. It should be noted that most of the studies reported so far were carried out either on model catalysts (single crystal or polycrystalline electrodes) or on realistic, however, not very well characterized fuel cell membrane electrode assemblies.

First results on the adsorption of ethanol and acetaldehyde on a commercial carbon-supported Pt fuel cell catalyst in a well-defined thin-film electrode configuration, measuring the current transients upon adsorption under controlled mass transport and detecting the desorption products by differential electrochemical mass spectrometry (DEMS), were published recently.[12] In the present paper, we focus on the continuous (bulk) ethanol oxidation over a Pt/Vulcan catalyst under continuous mass transport conditions, in particular the current efficiencies and product yields for CO_2, acetaldehyde, and acetic acid formation under different reaction conditions, which are calculated on the basis of DEMS measurements in a dual flow-through cell after proper calibration of corresponding mass signals.

In the following we will, after a brief description of the experimental setup and procedures, first evaluate the product yield and current efficiencies for CO_2, acetaldehyde, and acetic acid on a carbon-supported Pt/Vulcan catalyst at room temperature and for 0.1 M ethanol solution (section 3.1), then focus on the effects of ethanol concentration (0.001−0.5 M, section 3.2) and reaction temperature (23−60 °C, section 3.3), and in section 3.4 evaluate the effect of catalyst loading/electrode roughness by comparison with similar DEMS measurements on a smooth polycrystalline Pt electrode.

The results show that incomplete oxidation products are predominant, regardless of ethanol concentration, reaction temperature, or the nature of the catalyst, whereas the activity for complete ethanol electrooxidation to CO_2 under experimental conditions employed here is low. They also demonstrate that Pt/Vulcan anode catalysts are not attractive for low-temperature operation of a direct ethanol fuel cell due to the emission of toxic byproducts.

2. Experimental Section

DEMS Setup and the Experimental Details. The DEMS setup, which consisted of two differentially pumped chambers, a Balzers QMS 112 quadrupole mass spectrometer, a Pine Instruments potentiostat and a computerized data acquisition system, had been described in more detail previously.[16]

The thin-film Pt/Vulcan (20 wt % metal, E-TEK Inc.) electrodes for the DEMS measurements were prepared following the procedure described in ref 17, by pipetting and drying 20 μL of aqueous catalyst suspension (2 mg/mL) and then 20 μL of aqueous Nafion solution in the center of mirror-polished glassy carbon disks (Sigradur G from Hochtemperatur Werkstoffe GmbH, 9 mm in diameter). The resulting catalyst thin film had a diameter of ca. 6 mm, a geometric surface area of 0.28 cm^2, and a Pt loading of 28 $\mu g/cm^2$. A polished polycrystalline Pt disk (Mateck) 9 mm in diameter was used as a working electrode for comparative studies.

The electrode was mounted into a dual thin-layer flow-through DEMS cell[18] and pressed against a ca. 50 μm thick spacer. This leaves an exposed area of 0.28 cm^2 and results in an electrolyte volume of ca. 5 μL at the working electrode. The electrolyte flow was driven by the hydrostatic pressure in the supply bottle (flow rate about 5−6 μL/s), which ensures a fast transport of the species formed at the electrode to the mass spectrometric compartment, where the volatile products were evaporated into the MS (time constant, ca. 2 s) through a bare porous membrane (Scimat, 60 μm thick, 50% porosity, 0.2 μm pore diameter). Two Pt wires at the inlet and outlet of the thin-layer cell, connected through an external resistance (1 MΩ), were used as the counter electrodes. A saturated calomel electrode (SCE), connected to the outlet of the DEMS cell through the Teflon capillary, served as a reference electrode. All potentials, however, are quoted against the reversible hydrogen electrode (RHE).

The supporting electrolyte was prepared using Millipore Milli Q water and ultrapure sulfuric acid (Merck, suprapur). Ethanol (LiChrosolv) was obtained from Merck, and CO (N4.7) from Messer-Griesheim. Before measurements all solutions were deaerated by high-purity Ar (MTI Gase, N6.0). All experiments were carried out at room temperature (23 ± 1 °C), except for the elevated temperature DEMS experiments.

Elevated Temperature DEMS Measurements. To achieve a well-defined temperature control for the elevated temperature DEMS measurements, the whole DEMS cell assembly was mounted into an air thermostat. This is a double-walled stainless steel cube with isolation material between the steel plates. The inner side walls are heated by four heater plates (16 W each) up to the desired temperature, which is monitored via a Pt-100 thermocouple and controlled by an external home-built electronic unit to an accuracy of at least ±0.5 °C within the temperature range 25−80 °C (the calibration between the set temperatures and those achieved inside the thermostat was performed in advance). The air thermostat was closed tightly at the top of the box by mounting a double-walled stainless steel lid with a single 6 mm opening to connect the all-glass tip of the water-jacketed electrolyte supply bottle to the exactly positioned inlet of the DEMS cell. The electrolyte in the supply bottle was thermostated (±0.1 °C) separately using a water thermostat (Lauda E200). The DEMS cell was connected to the ultrahigh vacuum system by an extension piece, which passes through a fit-tight opening at the double-walled bottom of the thermostated box. All connections to the DEMS cell (two Pt-wire counter electrodes, reference electrode, separate inlet for CO adsorption, and solution outlet) were extended by Teflon capillaries through small holes to be freely accessible outside the thermostated box, so that all the procedures (CO adsorption, flushing of the connecting capillaries, etc.) were conducted without loss of potential and temperature control and without opening the thermostated box. An external and thermally fully decoupled SCE reference electrode, which was always kept at room temperature, allowed us to avoid corrections for temperature-induced potential shifts.[5,19]

Calibration of the DEMS Setup. To avoid any interference between CO_2^+ and CH_3CHO^+ ion currents (both at $m/z = 44$), which are the major ethanol electrooxidation products, the formation of carbon dioxide and acetaldehyde was monitored at $m/z = 22$ (doubly ionized CO_2^{2+}, 2.8% of the main $m/z = 44$ CO_2 peak) and $m/z = 29$ (COH^+ main fragment, 220% of the $m/z = 44$ acetaldehyde peak), respectively. The average current efficiency for complete ethanol electrooxidation to CO_2 per one carbon atom ($6e^-$ per CO_2 molecule) was calculated using the following equation:

$$A_q(CO_2) = 6Q_i/(K^*_{22}Q_f) \quad \text{or} \quad A_i(CO_2) = 6I_i/(K^*_{22}I_f) \quad (1)$$

where Q_f and I_f are the Faradaic charge and Faradaic current during ethanol oxidation, respectively, and Q_i and I_i are the corresponding mass spectrometric charge and current of $m/z = 22$. The factor of 6 reflects the number of electrons needed for formation of one CO_2 molecule from ethanol, K^*_{22} is the calibration constant for $m/z = 22$, found from CO_{ad} oxidation or CO bulk oxidation on a Pt catalyst. For CO_{ad} oxidation and CO bulk oxidation, respectively, K^*_{22} was calculated by

$$K^*_{22} = 2Q_i/Q_f \quad \text{or} \quad K^*_{22} = 2I_i/I_f \quad (2)$$

where Q_f and I_f are the Faradaic charge and Faradaic current during CO_{ad} oxidation and CO bulk oxidation, respectively, and Q_i and I_i are the corresponding mass spectrometric charge and current of $m/z = 22$, 2 is the number of electrons needed for formation of one CO_2 molecule from CO_{ad} or CO bulk. Such calibration for bulk CO electrooxidation was performed for both $m/z = 44$ and $m/z = 22$ at each temperature to evaluate the changing ionization probabilities for single and doubly ionized CO_2 molecules at increasing temperature, due to an increasing water vapor pressure in the mass spectrometer chamber.

The current efficiency of acetaldehyde formation was calculated using the following equation:

$$A_q(CH_3CHO) = 2Q_i/(K^*_{29}Q_f) \quad \text{or} \quad A_i(CH_3CHO) = 2I_i/(K^*_{29}I_f) \quad (3)$$

where K^*_{29} was found from the selective oxidation of ethanol to acetaldehyde on Au electrode at the high potential (>1.6 V) and the high concentration of ethanol (>0.5 M), because the current efficiency of acetaldehyde formed on the Au electrode under these conditions is about 90%:[20]

$$K^*_{29} = 2 \times I_i/(I_f^* \times 0.9) \quad (4)$$

Acetic acid formation could not be directly detected due to its low vapor pressure, and ethyl acetate ester formation could be detected (through $m/z = 61$ fragment[1]) in the negative-going scan only at high (0.5 M) ethanol concentration. Therefore, acetic acid yields were determined indirectly, calculating the difference between the measured Faradaic current and the partial currents for ethanol oxidation to CO_2 and acetaldehyde, which were found from the corresponding ion currents as described above. This calculation is based on the assumption that only three reaction products, namely CO_2, acetaldehyde, and acetic acid, are formed during ethanol oxidation.

The individual product yields ($W_{q,i}$) were calculated from the corresponding current efficiencies ($A_{q,i}$) through

$$W_{q,i} = (A_{q,i}/n_i)/\sum_i A_{q,i}/n_i \quad (5)$$

where n_i is the electron number in the ethanol oxidation reaction to the corresponding product (2 per acetaldehyde, 4 per acetic acid, and 6 per CO_2 molecule formation, respectively). The average number of electrons (n_e) produced per molecule in the ethanol electrooxidation reaction was estimated from the corresponding product current efficiencies as

$$n_e = 1/\sum_i A_{q,i}/n_i \quad (6)$$

respectively. In addition, we have monitored qualitatively the formation of methane and ethane at low potentials (0.06−0.3 V) via the mass signals $m/z = 15$ (CH_3^+ fragment of methane) and $m/z = 30$ (molecular ion of ethane, $C_2H_6^+$).

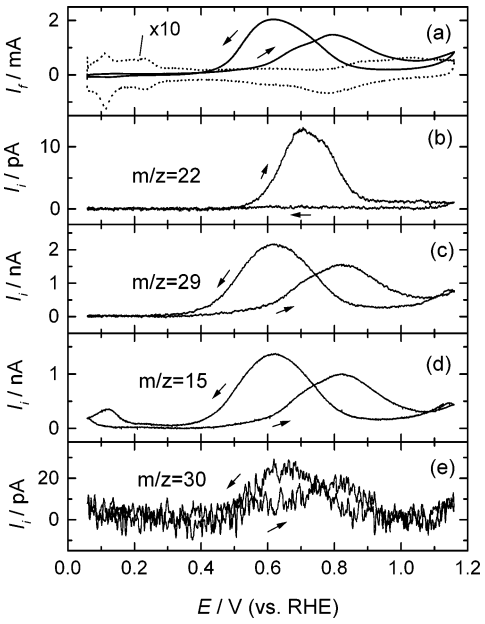

Figure 1. Simultaneously recorded CVs (a) and MSCVs for $m/z = 22$ (b), $m/z = 29$ (c), $m/z = 15$ (d), and $m/z = 30$ (e) of the ethanol oxidation reaction on a Pt/Vulcan catalyst in 0.1 M ethanol + 0.5 M H_2SO_4 solution. Scan rate: 10 mV/s, room temperature. Arrows indicate the direction of the potential scan. The dotted line (a) shows the base CV of Pt/Vulcan catalyst in 0.5 M H_2SO_4 solution.

3. Results and Discussion

3.1. Ethanol Oxidation on a Pt/Vulcan Catalyst at Room Temperature and 0.1 M Ethanol Concentration. *3.1.1. Cyclic Voltammetry DEMS Measurements.* The results of room-temperature DEMS measurements on the potentiodynamic ethanol electrooxidation over the Pt/Vulcan catalyst in 0.1 M ethanol containing 0.5 M H_2SO_4 solution at room temperature are shown in Figure 1. They include the (Faradaic current) cyclic voltammogram (CV) (a) and the corresponding mass spectrometric cyclic voltammograms (MSCVs) for the ion currents $m/z = 22$ (b), $m/z = 29$ (c), $m/z = 15$ (d), and $m/z = 30$ (e).

The steady-state cyclic voltammogram for ethanol electrooxidation on the Pt/Vulcan catalyst, recorded after several cycles (Figure 1a), largely resembles the characteristic current−voltage features reported for ethanol oxidation on polycrystalline Pt electrodes.[3,8,14,21] Electrooxidation of ethanol at potentials below ca. 0.4 V is largely blocked by adsorbed poisoning intermediates (CO and hydrocarbon residues[12]). It occurs at an appreciable rate only at potentials positive of ca. 0.5 V, where these species can be removed oxidatively, resulting in an ill-resolved double peak in the positive-going scan. At higher potentials (>0.8 V) ethanol oxidation is hindered by PtO formation. It should be

noted that at potentials positive of 1.1V the ethanol oxidation current starts to increase again. A similar increase is known from ethanol oxidation on polycrystalline Pt, where it results in a second oxidation peak (see section 3.4).[6−8,14,21] This peak is hardly visible here because we did not exceed 1.2 V in our experiments to avoid electrooxidation of the carbon support.[22] In the negative-going scan ethanol oxidation currents set in with the reduction of the platinum oxide negative of ca. 0.85 V and decrease again at more negative potentials due to repoisoning of the catalyst. The interplay of these factors results in different potentials of the corresponding anodic current peak maxima for positive- and negative-going scans.

For more product specific information we also monitored the mass spectrometric signals for CO_2 and for acetaldehyde formation via the doubly ionized molecular ion signal at $m/z = 22$ (Figure 1b) and the acetaldehyde related signal at $m/z = 29$ (see section 2). The onset of CO_2 formation in the positive-going scan of the steady-state voltammogram occurs at ca. 0.5 V (Figure 1b). With increasing potential it equally results in an ill-resolved double peak for CO_2 formation with maxima at ca. 0.7 and 0.78 V. Note that the first peak for CO_2 formation, which corresponds to the first peak in the Faradaic current (Figure 1a), is higher than the second one in the mass spectrometric signal, whereas in the Faradaic current signal it is lower than the second one. The Faradaic current in the range of the first peak results to a significant extent from the partial reaction current for CO_2 formation. The second peak in the Faradaic current is mainly attributed to acetaldehyde and acetic acid formation.

Because we had obtained comparable amounts of CO_2 as observed upon ethanol adsorbate stripping (including corrections for the difference between CO_2^+ and CO_2^{2+} intensity), and because during ethanol adsorption at potentials <0.45 V CO_{ad} is the main, stable adsorbate,[12] we conclude that CO_2 formation results from the oxidation of adsorbed CO. The latter was formed at potentials <0.6 V, negative of the CO_2 peak, in the preceding negative-going scan and in the low potential part of the positive going scan. CO_{ad} formation in the range of the CO_2 peak is possible as well, but the total amount is limited due to the short time spent in this range and the relatively slow rate. Therefore, the total amount of CO_{ad} formed between 0.6 and 1.0 V is small but existent, which is reflected by the somewhat broader CO_2 signal as compared to the CO_2 formation during ethanol adsorbate stripping.[12] Because of the different height of the second peak relative to the first one, we conclude that this includes formation of other ethanol oxidation products, in addition to CO_2 formation. At potentials positive of 0.9 V the CO_2 formation rate in the positive-going scan drops to a low, constant value, despite the increase in Faradaic current at the positive potential limit (Figure 1a). In the negative-going scan, CO_2 formation is completely suppressed over the entire potential range (Figure 1b), although the Faradaic current exhibits a distinct peak centered at ca. 0.6 V (Figure 1a). This result agrees well with previous DEMS data obtained on sputtered Pt electrode,[14,23] and suggests already predominant formation of incomplete ethanol oxidation products (acetaldehyde and acetic acid) in the negative-going scan (see below). The suppression of CO_2 formation for ethanol oxidation in the negative-going scan can be explained by a low C−C bond splitting rate at potentials positive of about 0.5 V, whereas at lower potentials, where C−C bond dissociation and subsequent CO_{ad} formation is more facile, CO_{ad} oxidation is hindered by the lack of OH_{ad} species. One may speculate that at potentials >0.5 V C−C bond splitting is inhibited by the presence of OH_{ad} species.

As described in the Experimental Section, monitoring the CHO^+ fragment of acetaldehyde at $m/z = 29$ (Figure 1c) allows us to avoid interference with the CO_2 signal at $m/z = 44$, which occurs for the molecular ion of acetaldehyde, and thus to detect acetaldehyde formation selectively during incomplete ethanol electrooxidation. It should be noted that discrimination between the two ethanol oxidation products can also be achieved by using fully deuterated ethanol, resulting in a corresponding shift of the main acetaldehyde peak by four mass numbers.[2,14,23] However, in addition to being more expensive, this approach may involve kinetic isotope effects for ethanol C−D bond splitting as compared to C−H bond breaking, and thus can result in slower electrooxidation kinetics. In addition, on-line detection of acetaldehyde using DEMS combined with a flow cell is favorable compared to long-term kinetic experiments involving ethanol electrooxidation and product analysis using chromatographic techniques,[8] because of the possible losses of acetaldehyde in an open system, due to high volatility of acetaldehyde (low boiling temperature).

Several important features are observed for acetaldehyde formation as a function of electrode potential (Figure 1c): (i) The onset of acetaldehyde formation in the positive-going scan occurs at potentials positive of ca. 0.35 V, simultaneously with the onset of ethanol oxidation (Figure 1a). In combination with the absence of CO_2 formation at potentials below 0.4 V (Figure 1b), this suggests preferential incomplete oxidation of ethanol at low potentials, in agreement with previous IR data.[21,24] (ii) Passing the first maximum in the Faradaic current double peak acetaldehyde formation continues to increase and finally results in a peak at ca. 0.8 V. The potential of this latter peak corresponds to that of the second anodic current peak. At higher potentials the $m/z = 29$ signal follows the Faradaic current signal (Figure 1a) (please note that the shift by ca. 20 mV for the mass spectrometric signal is due to the time constant of the flow-cell of ca. 2 s). Together with the constant, low CO_2 formation rate at these potentials (Figure 1b) this implies that incomplete ethanol oxidation (to acetaldehyde and acetic acid) prevails also at more positive potentials, in agreement with previous IR observations.[7,21] (iii) In the negative-going scan (Figure 1c), acetaldehyde formation follows the Faradaic current (Figure 1a), with a dominant peak in both signals centered at ca. 0.62 V. Under these conditions, where CO_2 formation was barely measurable (Figure 1b), ethanol oxidation proceeds exclusively to incomplete oxidation products. The current efficiency for acetaldehyde and acetic acid formation in the negative-going scan could be estimated ca. 37% and 63%, respectively, at a negligible ($<1\%$) current efficiency for CO_2 formation (a detailed discussion of current efficiencies and product yields will be given in section 3.2). In contrast, for ethanol electrooxidation on Pt(111) acetic acid was found to be the predominant product in the negative-going scan according to IR observations.[7] We tentatively attribute this difference to an experimental artifact in the previous IR measurements caused by the thin-layer geometry: In those experiments acetaldehyde being trapped in the thin layer of electrolyte between the electrode and the prism in a thin-layer IR configuration may readsorb and further oxidized to acetic acid, whereas under the continuous flow conditions in our experiments intermediate ethanol oxidation products are continuously removed.

The other major ionic fragment from acetaldehyde decomposition is CH_3^+, which results in the ion current at $m/z = 15$ (Figure 1d). This signal exactly follows the features of $m/z = 29$ ion current (Figure 1c) at potentials positive of 0.3 V, indicating that both ions result from the same parent molecule

(H_3C-CHO). However, in contrast to the featureless shape of the $m/z = 29$ signal at potentials below 0.3 V (Figure 1c), the $m/z = 15$ ion current displays new features during the negative-going scan at these potentials (Figure 1d). These are attributed to cathodic methane formation, in agreement with previous data obtained on a porous Pt electrode.[2] Qualitatively and quantitatively similar methane formation characteristics were observed after (dissociative) ethanol adsorption at 0.66 V on a Pt/Vulcan catalyst in the subsequent negative-going scan in the H_{upd} region,[12] suggesting that also in ethanol-containing solution methane is formed by cathodic reduction of the adsorbed species at potentials <0.3 V, most likely of hydrocarbon residues, rather than by bulk reduction of ethanol to methane. Additional evidence for that hypothesis will be presented later (see chapters 3.2−3.4)

Similarly to methane, cathodic formation of ethane can be monitored trough the $m/z = 30$ ion signal at potential below 0.3 V (Figure 1 e). At more positive potentials the $m/z = 30$ ion current is dominated by the isotopically shifted (resulting from the natural abundance of the ^{13}C, ^{17}O, and ^{2}H isotopes) COH^+ fragment, which can be concluded from the similar shape of the $m/z = 30$ and the $m/z = 29$ mass signals (Figure 1c) at potentials positive of 0.3 V. Cathodic ethane production from ethanol is barely detectable on a Pt/Vulcan catalyst (Figure 1e) and constitutes only 2−5% of the amount of methane formation (Figure 1d), in contrast to the ca. 50% ethane reported in the literature for a sputtered porous Pt electrode.[2] We found recently that continuous reduction of acetaldehyde to ethane occurs at 0.06 V on a Pt/Vulcan catalyst.[25] Therefore, the low cathodic ethane yields from ethanol in our potentiodynamic experiments compared to previous data[2] are tentatively explained by the continuous removal of the volatile reaction intermediate/side product acetaldehyde under flow-through conditions in our experiments, which is not possible in the stagnant electrolyte used in the previous experiments. Other experimental differences such as the difference in Pt catalyst (carbon-supported Pt nanoparticles vs sputtered Pt), the different supporting electrolyte (sulfuric acid solution in our case and perchloric acid solution in ref 2), or the difference in negative potential limit (0.06 V in our case and 0 V in ref 2), may also play a role, but we think that these are second-order effects.

3.1.2. Potentiostatic DEMS Measurements. In the second part we report results of potentiostatic DEMS measurements monitoring the ethanol electrooxidation transients upon stepping the potential to 0.61 V, which would be a typical (though economically undesirable) potential for stable fuel cell operation (Figure 2). Similarly to the above measurements we followed the Faradaic current transients (Figure 2a) and the mass spectrometric current signals for CO_2 (Figure 2b) and acetaldehyde (Figure 2c), and calculated the current efficiencies for CO_2 (Figure 2d) and acetaldehyde (Figure 2e) formation. Two sets of experiments were carried out using different initial potentials, prior to the potential step, namely 0.06 (gray lines) and 0.26 V (black lines), respectively. The first situation corresponds to a "clean" Pt surface, considering that ethanol adsorption is inhibited on a H_{upd}-covered surface, and the second to a Pt surface covered by a mixed adlayer of CO_{ad} and hydrocarbon residues (total coverage ca. 0.5 relative to a saturated CO adlayer). This adlayer is developed due to dissociative ethanol adsorption on the Pt surface, which is possible because of the very low H_{upd} coverage.[12] For removal of adsorbed species before going to the initial potential, either 0.06 or 0.26 V, the electrode was biased for ca. 30 s at a potential of 1.1 V (platinum oxidation region).

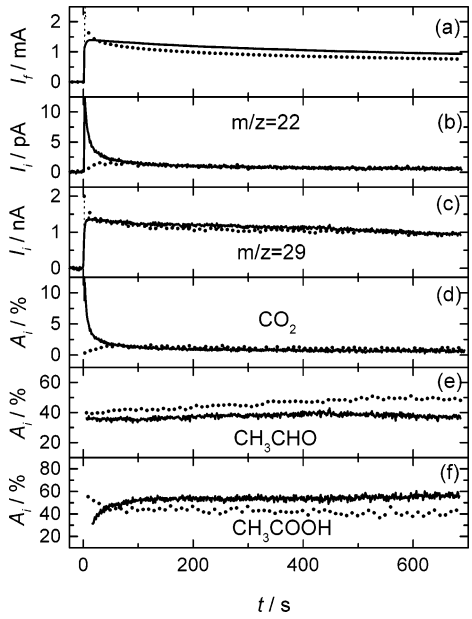

Figure 2. Simultaneously recorded transients of the Faradaic current (a) and the ion currents for $m/z = 22$ (b) and $m/z = 29$ (c) for ethanol oxidation on a Pt/Vulcan catalyst in 0.1 M ethanol + 0.5 M H_2SO_4 solution after a potential step from 0.06 to 0.61 V (dotted), or from 0.26 to 0.61 V (black). (d)−(f) show the current efficiencies for CO_2, CH_3CHO, and CH_3COOH formation, respectively.

After stepping the electrode potential from 0.06 to 0.61 V (Figure 2a, dotted line) the Faradaic current transient displays a sharp increase to 3 mA, followed by an approximately exponential decay in current down to ca. 0.8 mA. For the potential step from 0.26 to 0.61 V (Figure 2a, black line) the Faradaic current also increases abruptly, but only to ca. 1.2 mA, and then passes through a smooth maximum after ca. 10 s (maximum current about 1.4 mA). It then steadily decays with time to ca. 0.9 mA. The pronounced difference in the initial current transient behavior for the two different initial potentials can be rationalized as follows: When stepping from 0.06 to 0.6 V (starting from a completely H_{upd}-blocked surface that is free of adsorbed ethanol decomposition products), the Faradaic current transient results from several contributions, namely, (i) instantaneous oxidation of the H_{upd} adlayer, (ii) simultaneous dissociative adsorption of ethanol (see section 3.2), (iii) pseudocapacitive currents, and (iv) the onset of ethanol bulk oxidation, all contributing to the sharp Faradaic current spike. The rapid development of poisoning adspecies (adsorbed CO and hydrocarbon residues) due to dissociative ethanol is responsible for the rapid decay of the Faradaic current. In the second case, for the potential step from 0.26 to 0.61 V, the catalyst surface is initially covered by a mixed adlayer consisting of CO_{ad} and adsorbed hydrocarbon residues,[12] and therefore the initial current transient is governed by the relatively slow electrooxidation of adsorbed poisoning species and by the onset of bulk ethanol oxidation.

This interpretation is supported by the simultaneous DEMS measurements of the mass spectrometric transients for CO_2 formation (Figure 2b). For the potential step from 0.06 to 0.61 V (dotted line) we do not observe a spike similar to that exhibited by the Faradaic current, but a sudden step in intensity followed by a smooth increase to a shallow maximum for CO_2 formation. This maximum is significantly later than that of the Faradaic current transient, by ca. 20−30 s, which is considerably more than the response time of the dual flow cell (1−2 s). The slow initial increase can be explained by the electrooxidation of CO_{ad} intermediates, which are developed *after* the potential

step. In contrast, for the potential step from 0.26 to 0.61 V the $m/z = 22$ ion current transient shows an immediate increase to a ca. 10-fold higher value, and a subsequent steep decrease (Figure 2b, black line); i.e., in this case we find a sharp spike, which for the Faradaic current was observed after stepping from 0.06 to 0.61 V. This is explained by the oxidation of adsorbed CO present prior to the potential step. Finally, after almost 100 s, the $m/z = 22$ signal assumes an almost constant steady-state value, which is independent of the initial potential and hence of the initial condition of the surface. Comparing this signal with those obtained from CO stripping experiments the constant CO_2 signal corresponds to a CO_{ad} oxidation rate of about 1×10^{-3} monolayer/s. The slow decrease in CO_2 formation with time in both cases can be explained by the progressing catalyst surface poisoning due to accumulation of poisoning species different from CO_{ad}. Our recent DEMS measurements on a Pt/Vulcan catalyst had shown that continuous ethanol oxidation at 0.65 V leads to the formation of adsorbates that develop methane in the H_{upd} region during a subsequent negative-going scan. Going to more positive potentials, these adsorbates can be oxidized to CO_2 at potentials positive of 0.9 V.[12] Such gradual poisoning of the catalyst by species that cannot be oxidized at low potentials can explain also the observed decrease in the Faradaic current for ethanol oxidation with time (Figure 2a).

Acetaldehyde formation after the potential step from 0.06 to 0.61 V (Figure 2c, gray line) largely follows the behavior of the Faradaic current, with a sharp spike on the initially "clean" surface and an abrupt increase to a value slightly higher than the steady-state current and a subsequent slow decay on the partly blocked catalyst, after stepping from 0.26 to 0.61 V (Figure 2c, black line). The high current signal on the 'clean' catalyst, however, decays rapidly, and attains approximately the same value as that on the partly blocked catalyst. As discussed before, the initially high rate and the subsequent rapid decay can be explained by a rapid development of poisoning species (adsorbed CO and hydrocarbon residues) due to ethanol dissociative adsorption.[12] Comparing the Faradaic current transient with that for methanol oxidation after a potential step from 0.06 to 0.61 V on the same catalyst and under the same conditions (catalyst loading, alcohol concentration, temperature and electrolyte flow rate) on a Pt/Vulcan catalyst,[26] we find similar steady-state currents in both cases (Figure 2a), whereas the steady-state CO_2 production during ethanol electrooxidation is by about 1 order of magnitude lower than that for methanol oxidation. This indicates prevailing incomplete ethanol oxidation in contrast to a dominant complete methanol oxidation under these conditions.

Finally, we quantitatively determined the current efficiencies for ethanol oxidation product formation as described in chapter 2.3, assuming that CO_2, acetaldehyde, and acetic acid are the only reaction products. For the potential step from 0.06 to 0.61 V (Figure 2d−f, dotted lines) the current efficiency for ethanol electrooxidation products slightly varies with time, changing from 39 to 49% for acetaldehyde, from 60 to 50% for acetic acid, and between 1 and 1.5% for CO_2. Coming from 0.26 V starting potential (Figure 2d−f, black lines), the apparent current efficiency for CO_2 formation is initially very high, but then decays to 1.5−1%. The apparently high current efficiency in the initial phase is caused by the oxidation of preadsorbed CO-type species right after the potential step, due to the only 2 electrons per CO_{ad} oxidation vs 6 electrons per CO_2 molecule formation for complete ethanol oxidation. Under steady-state conditions the current efficiencies for acetaldehyde and for acetic acid formation are rather similar to those obtained for 0.06 V starting potential, slowly increasing from 35 to 40% for the former and being around 60% for the latter. The somewhat lower current efficiency for acetaldehyde on this surface than on the "clean" (0.06 V starting potential) is tentatively attributed to the presence of $CH_{x,ad}$ species, which cannot be oxidized at this potential and thus reduce the rate for acetaldehyde formation.

Summarizing these findings, acetaldehyde (57−67%) and acetic acid (43−33%) are the predominant products for ethanol oxidation at 0.61 V in 0.1 M solution, the CO_2 yields being below 1%, taking into account the difference in the number of electrons gained for ethanol electrooxidation to the respective reaction products (2 per acetaldehyde, 4 per acetic acid, and 6 per CO_2 molecule formation, respectively). Similar trends were reported for ethanol electrooxidation on polycrystalline Pt at 0.6 V (0.025 M ethanol in 0.1 M $HClO_4$ solution, temperature 10 °C), with selectivities of 90 and 10% for acetaldehyde and acetic acid formation.[8] The higher acetic acid yields at 0.6 V in our experiments can be understood from the higher ethanol concentration (see chapter 3.2), reaction temperature (see section 3.3), and electrode roughness (see chapter 3.4). Acetic acid is formed either directly by adsorbed ethanol oxidation, in a second step after reaction to an adsorbed acetaldehyde-type species, or via desorption and subsequent readsorption/oxidation of the intermediate product acetaldehyde. Readsorption can occur at this catalyst loading even under continuous flow of electrolyte, whereas it is much less likely on a smooth electrode (cf. methanol oxidation[26]). Only trace amounts of CO_2 are produced, presumably via oxidation of adsorbed CO species formed as a result of ethanol C−C bond splitting. Hence, the final reaction step, oxidation of acetic acid to CO_2, is kinetically inhibited at this potential and temperature, which agrees well with previous literature reports[5] and with the results of recent DEMS measurements on acetic acid oxidation in our laboratory.[27] Those data showed that acetic acid oxidation on Pt electrodes/catalysts is only possible at elevated temperatures.

3.2. Ethanol Concentration Effects on the Electrooxidation Product Yields and Current Efficiencies. To evaluate the influence of ethanol concentration on current efficiencies and electrooxidation product yields, we performed a series of cyclic voltammetry DEMS measurements at different ethanol concentrations (0.001, 0.01, and 0.5 M) on a Pt/Vulcan catalyst at room temperature, analogous to those shown for 0.1 M ethanol solution in Figure 1. Figure 3 shows a representative data set for 0.01 M ethanol solution. After exchange of supporting electrolyte to ethanol containing solution at 0.06 V, the first positive-going scan (Figure 3a, dotted line) exhibits a more pronounced anodic current peak at ca. 0.25 V compared to the base CV of the Pt/Vulcan catalyst (Figure 1, dotted line), which is not present in the CO_2 formation signal (Figure 3b, dotted line). Similar observations were reported for ethanol oxidation on sputtered Pt electrodes.[8] This can be attributed to instantaneous adsorption of ethanol residues, which can occur on the partly H_{upd}-covered Pt surface at $E > 0.06$ V during the positive-going scan, whereas on the fully H_{upd}-blocked surface ($\theta_H = 0.77$ monolayer at 0.06 V) ethanol adsorption is largely inhibited.[12]

The steady-state cyclic voltammogram for ethanol oxidation in 0.01 M solution (Figure 3a, solid line) closely resembles that obtained in 0.1 M solution (Figure 1a) in its general appearance. The Faradaic current peak is about 4 times lower in the positive-going scan and ca. 3 times lower in the negative-going scan compared to the corresponding anodic current peaks for 0.1 M ethanol solution (Figure 1a). Hence, the decrease in ethanol concentration by 1 order of magnitude (0.1 to 0.01 M) causes

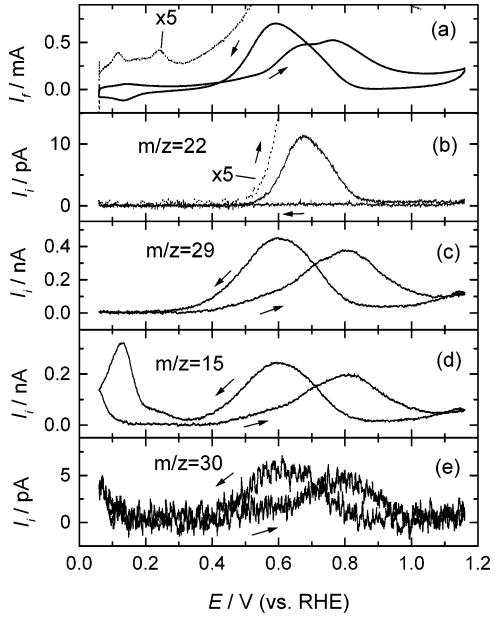

Figure 3. Simultaneously recorded CVs (a) and MSCVs for m/z = 22 (b), m/z = 29 (c), m/z = 15 (d), and m/z = 30 (e) for ethanol oxidation on Pt/Vulcan catalyst in 0.01 M ethanol + 0.5 M H_2SO_4 solution. Scan rate: 10 mV/s, room temperature. Arrows indicate the direction of the potential scan. Dotted lines (a, b) show the first positive-going scan.

a ca. 4-fold decrease in oxidation current. This result indicates that the overall electrooxidation rate is controlled by surface processes rather than by pure mass transport.

The first Faradaic current peak at ca. 0.65 V in the positive going-scan in 0.01 M solution is better resolved here than in 0.1 M ethanol solution (Figure 1a). As discussed before, it mainly results from the oxidation of adsorbed species (Figure 3b). This conclusion is supported by the fact that the maximum m/z = 22 signal is about the same for 0.01 and 0.1 M ethanol solution, as would be expected for oxidation of surface species at a similar coverage, but not for bulk electrooxidation reaction. Acetaldehyde formation (m/z = 15, 29) is decreased by a factor of about 5 in 0.01 M ethanol solution (Figure 3d), compared to 0.1 M ethanol solution (Figure 1c,d). The amount of methane (m/z = 15) produced by cathodic desorption at <0.3 V in 0.01 M ethanol solution is similar to that in 0.1 M ethanol solution (Figures 3d and 1d), implying a comparable coverage of adsorbate developed for different ethanol concentrations. Finally, ethane formation is more clearly resolved in 0.01 M ethanol solution (Figure 3e) than in 0.1 M solution, which is mainly attributed to the lower background signal at this mass number because of the lower ethanol vapor pressure.

To quantify the product yields and calculate the current efficiencies for the ethanol oxidation products CO_2, acetaldehyde, and acetic acid at different ethanol concentrations (0.001, 0.01, 0.1, and 0.5 M), we integrated the Faradaic current and the ion currents for CO_2 (m/z = 22) and acetaldehyde (m/z = 29) formation within a complete potential cycle (0.06 to 1.16 V and back to 0.06 V). The mass spectrometric charges were converted to electrochemical charges for CO_2 and acetaldehyde formation using the corresponding calibration constants (see Experimental Section). Finally, we calculated the net current (charge) for acetic acid formation as the difference between the net current and the sum of the two partial reaction currents (charges), assuming that CO_2, acetaldehyde and acetic acid are the only products for ethanol electrooxidation (minor contributions for cathodic desorption of methane were neglected).

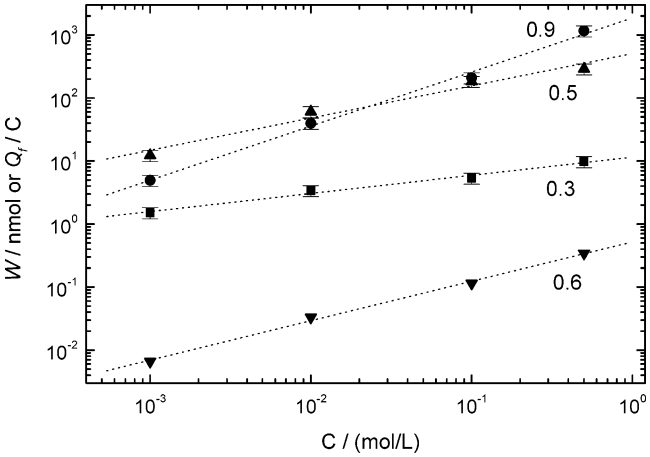

Figure 4. Total Faradaic charge (Q_f) and the amounts (W) of CO_2, acetaldehyde and acetic acid formed over a full cyclic scan as function of ethanol concentration: (■) CO_2; (●) acetaldehyde; (▲) acetic acid; (▼) total Faradaic charge.

Integrating the Faradaic charge and the mass spectrometric signals over the complete cycle has the advantage that the currents (charges) for all electrochemical processes are included, whereas on the other hand contributions from double-layer charging/discharging, hydrogen and oxygen adsorption/desorption cancel out. The disadvantage of this kind of treatment is that it does not allow us to evaluate potential effects on the different reactions.

Figure 4 shows a logarithmic plot for the absolute ethanol oxidation product yields, calculated along the above procedure. Assuming a simple exponential rate law, we can calculate the formal reaction order for ethanol from the slopes of the corresponding linear ln(charge) vs ln(concentration) dependences. The formal reaction order for the total Faradaic charge of 0.6 is comparable to the value of 0.7 determined from the cyclic voltammetric peak for ethanol oxidation at 0.8 V on a polycrystalline Pt electrode.[8] It should be noted that the reaction order found from the Faradaic current (charge) does not resolve details of the reaction mechanism and reaction kinetics, because it includes unspecified contributions of three different Faradaic processes. This is different for the partial reaction orders for acetaldehyde, acetic acid, and CO_2 formation determined in these DEMS experiments. They show a rather high reaction order of ca. 0.9 for the relatively simple ethanol oxidation to acetaldehyde. This reaction involves only two dehydrogenation steps and thus is likely to proceed with comparable efficiency also on a partly blocked catalyst surface, at higher ethanol concentrations. The lower reaction order for acetic acid formation of ca. 0.5 implies a more complex (surface) reaction scheme, as would be expected for reaction between OH_{ad} species and either adsorbed ethanol itself or an adsorbed acetaldehyde intermediate. The same is true for the even lower reaction order for CO_2 formation of 0.3. It should be noted that the reaction order for CO_2 formation refers mainly to the positive-going scan, because in the negative-going scan CO_2 formation is largely suppressed (see Figures 1b and 3b).

The relative product distributions (W) and average current efficiencies (A) for the formation of the different ethanol oxidation products (CO_2, acetic acid, and acetaldehyde) calculated from cyclic voltammetry DEMS data for different ethanol concentrations within one complete potential-scan cycle are compiled in Table 1. These demonstrate a pronounced dependence of the corresponding product yields and current efficiencies on the ethanol concentration. The relative amount of CO_2 decreases with ethanol concentration from about 7.5% at 0.001

TABLE 1: Average Current Efficiencies and Product Yields for CO_2, CH_3CHO, and CH_3COOH Formation over a Full Potential Cycle at Room Temperature as a Function of Ethanol Concentration

	C/mol L^{-1}			
	0.001	0.01	0.1	0.5
$A_q(CO_2)$/%	13	6.3	2.7	1.7
$W_q(CO_2)$/%	7.5	3.3	1.3	0.7
$A_q(CH_3CHO)$/%	15	26	37	66
$W_q(CH_3CHO)$/%	27	42	55	79
$A_q(CH_3COOH)$/%	72	68	60	32
$W_q(CH_3COOH)$/%	65	55	44	20

[a] A_q: average current efficiency. W_q: average product yield. C: the concentration of ethanol. The confidence interval is ca. 90%.

M ethanol concentration to ca. 0.7% at 0.5 M ethanol concentration, i.e., by always 1 order of magnitude. The same is true for the current efficiency for CO_2 formation, which decreases from ca. 13 to 1.7% with increasing ethanol concentration (0.001 to 0.5 M). Taking into account that (i) CO_2 formation in the positive-going scan mainly results from oxidation of preadsorbed ethanol decomposition products (see above) and that (ii) the total Faradaic current (charge) for ethanol oxidation decreases strongly with decreasing ethanol concentration (see Figures 1a and 3a), we conclude that the increase in the product yield and current efficiency for CO_2 formation at low ethanol concentration is only apparent, caused by the decrease in total ethanol oxidation current (charge). Hence, CO_2 is a minority product for ethanol oxidation on Pt/Vulcan catalysts at all concentrations investigated, whereas incomplete oxidation to the stable (soluble) reaction intermediates prevails.

The relative amount of acetaldehyde in ethanol electrooxidation products increases from ca. $^1/_5$ to $^4/_5$. Correspondingly, the relative amount of acetic acid decreases from ca. $^2/_3$ to $^1/_5$ with the increase in ethanol concentration from 0.001 to 0.5 M (Table 1). This results in an increase of the current efficiency for acetaldehyde formation from ca. 15 to 66%, whereas for acetic acid formation the current efficiency decreases from ca. 72 to 32% with increasing ethanol concentration. Hence, ethanol oxidation to acetic acid is favored over oxidation to acetaldehyde at low ethanol concentrations, whereas at higher concentrations acetaldehyde formation prevails. A possible explanation for this effect will be given in the next section. At this point we want to note that at the lower concentrations the steady-state concentrations of adsorbed reaction intermediates are also lower, which apparently favors oxidation to acetic acid on the expense of acetaldehyde formation.

Finally, a semilogarithmic plot of the resulting average numbers of electrons (n_e) per ethanol molecule oxidation, calculated (see chapter 2.3) from the corresponding current efficiencies (Table 1) as a function of ethanol concentration, shows a decrease of the average electron number from ca. 3.7 to 2.4 with increasing ethanol concentration, from 0.001 to 0.5 M (Figure 5).

These results are in a good agreement with the data reported previously on the basis of a chromatographic analysis of ethanol electrooxidation products on polycrystalline Pt electrode,[8] taking into account the different morphology of the Pt electrode (see chapter 3.4).

3.3. Temperature Effects on Ethanol Electrooxidation Product Yields and Current Efficiencies. To further investigate the kinetics of ethanol electrooxidation over Pt/Vulcan, we performed a series of cyclic voltammetry DEMS measurements at elevated temperatures (30, 40, 50, and 60 °C) in 0.01 M ethanol solution. For comparison we present DEMS data for

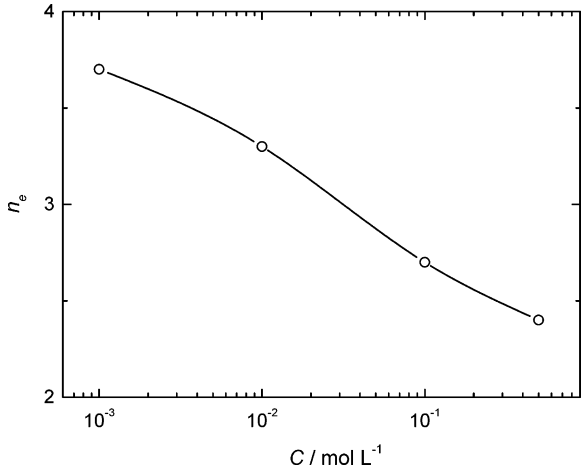

Figure 5. Average number of electrons per ethanol molecule oxidation integrated over a full cyclic scan versus the concentration of ethanol.

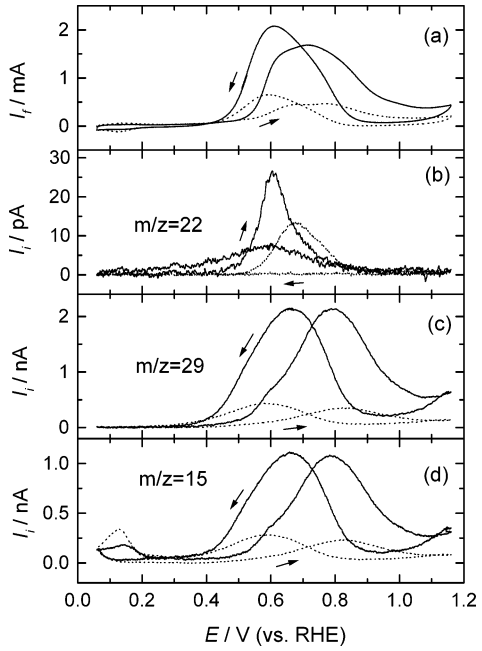

Figure 6. Simultaneously recorded CVs (a) and MSCVs for m/z = 22 (b), m/z = 29 (c), m/z = 15 (d) for ethanol oxidation on a Pt/Vulcan catalyst in 0.01 M ethanol + 0.5 M H_2SO_4 at different temperatures: (—) 60 °C; (···) 30 °C. Potential scan rate: 10 mV/s. Arrows indicate the direction of the potential scan.

30 °C (dotted lines) and 60 °C (full lines) respectively, in Figure 6. Note that for the present elevated temperature DEMS setup, which operates at atmospheric pressure, the temperature was limited to 60 °C due to evaporation of ethanol, which causes formation of bubbles in the extension capillaries and possible losses in electrical contact.

As evident from Figure 6a the Faradaic current for ethanol electrooxidation increases by a factor of about 4 when the temperature is raised from 30 to 60 °C. The maximum for CO_2 formation in the positive-going scan (Figure 6b, solid line) is shifted by ca. 0.1 V to more negative values at 60 °C, from 0.8 V at 30 °C (Figure 6b, dotted line) to 0.7 V at 60 °C. The peak in the CO_2 signal in the positive-going scan corresponds to a shoulder in the Faradaic current at the onset of ethanol electrooxidation (Figure 6a, solid line). Though CO_2 formation is negligible in the negative-going scan at 30 °C (Figure 6b, dotted line), appreciable amounts are formed during the negative-going scan at 60 °C. Considering our previous discussion

TABLE 2: Average Current Efficiencies and Product Yields for CO_2, CH_3CHO, and CH_3COOH Formation over a Full Potential Cycle as a Function of Temperature (0.01 M C_2H_5OH Solution)

	temp/°C			
	30	40	50	60
$A_q(CO_2)$/%	7.9	7.5	6.0	5.1
$W_q(CO_2)$/%	4.3	3.6	3.1	2.6
$A_q(CH_3CHO)$/%	26	30	32	35
$W_q(CH_3CHO)$/%	42	47	49	53
$A_q(CH_3COOH)$/%	66	63	62	60
$W_q(CH_3COOH)$/%	54	49	48	45

[a] A_q: the average current efficiency. W_q: the average yield. The confidence interval is ca. 90%.

(see section 3.1), this indicates that C−C bond splitting is activated at elevated temperatures. The rate for acetaldehyde formation is increased by about a factor of 5 for going from 30 °C (Figure 6c, dotted line) to 60 °C (Figure 6c, solid line). The sum of the partial currents for CO_2 and acetaldehyde formation at 60 °C (Figure 6c, solid line) deviates from the Faradaic current (Figure 6a, solid line). The misfit between the Faradaic current (Figure 6a, solid line) and the added currents for CO_2 (Figure 6b, solid line) and acetaldehyde (Figure 6c, solid line) formation indicates significant formation of acetic acid also at elevated temperatures.

Similar to its room-temperature characteristics the $m/z = 15$ mass signal (Figure 6d) traces acetaldehyde formation at potentials positive of 0.3 V and exhibits a slight increase in the negative going scan at potentials <0.3 V, which was attributed to cathodic desorption of adsorbed hydrocarbon residues formed at higher potentials.[12] Cathodic methane formation *decreases* with higher temperatures, shrinking to approximately one-half when going from 30 °C (Figure 6d, dotted line) to 60 °C (Figure 6d, solid line). In accord with the decrease in methane formation at higher temperatures we did not observe cathodic ethane desorption under these conditions ($m/z = 30$, not shown). This implies a significantly lower coverage of these ad-species at higher temperatures, which can be explained by taking into account that adsorbed hydrocarbon residues can be partly converted to CO_{ad}-type species due to a slow reaction with water.[10] Apparently, the latter reaction is accelerated at higher temperatures leading to formation of CO_{ad}-type species that can be oxidized at relatively lower overpotentials, compared to the oxidation of hydrocarbon residues which largely occurs in the PtO region.[12] In combination with the decrease in CO_{ad} coverage at elevated temperatures due to thermal desorption and the negative shift of the CO_{ad} oxidation peak,[27,29,30] the variation in the composition and the coverage of poisoning species will contribute to the significant increase in the overall ethanol oxidation rate with temperature (Figure 6a).

For a quantitative evaluation of the ethanol oxidation product yields and current efficiencies as a function of temperature, we integrated the Faradaic and corresponding mass spectrometric currents within a complete cycle as described in the previous chapter. The $m/z = 22$ ion signal was calibrated in continuous CO oxidation measurements on the Pt/Vulcan electrode for each temperature, whereas for $m/z = 29$ we used a constant calibration factor derived at room temperature, which was corrected for elevated temperatures by the same factor as determined for $m/z = 44$ in bulk CO oxidation measurements at the corresponding temperatures. The resulting values for the corresponding ethanol oxidation product yields and current efficiencies are listed in Table 2. The current efficiencies decrease from 8% to 5% for CO_2 and from 66% to 60% for acetic acid formation for increasing the temperature from 30 to 60 °C, whereas for acetaldehyde formation increases with temperature from 26% to 35%. The corresponding product distribution with increasing temperature from 30 to 60 °C shows a decrease in the CO_2 and acetic acid product yields from 4% to 2.5% and from 54 to 45%, respectively, whereas the acetaldehyde product yield increases from 42% to 53%.

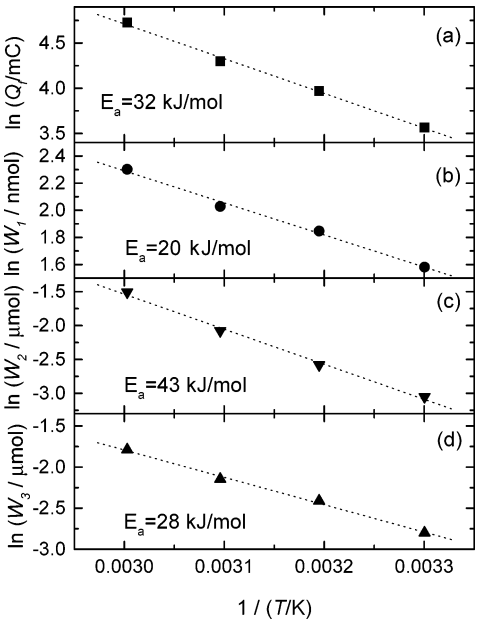

Figure 7. Total Faradaic charge (Q_f) and the amounts of CO_2 (W_1), acetaldehyde (W_2), and acetic acid (W_3) formed in a full potential cycle as a function of temperature for ethanol oxidation on a Pt/Vulcan catalyst in 0.01 M ethanol + 0.5 M H_2SO_4.

From the linear slopes of the integrated charges in the Arrhenius plots in Figure 7 we determined the averaged apparent activation energies (E_{app}) for the overall ethanol electrooxidation reaction (Figure 7a) and for the partial reactions for the formation of the individual reaction products CO_2 (Figure 7b), acetaldehyde (Figure 7c), and acetic acid (Figure 7d). Commonly, the apparent activation energies are determined from the Faradaic current/charge (see, e.g., refs 19 and 29 as examples for methanol oxidation), which yields a nonspecific average value resulting from several contributing reactions (here, e.g., ethanol oxidation to acetaldehyde, acetic acid, and CO_2). In contrast, the present DEMS experiments allow us to get direct access to the activation energies for the partial reactions. It should be noted that the values for the apparent activation energies for the partial reactions may include also contributions from the oxidation of poisoning adsorbed hydrocarbon residues (see Figure 6d), which is possible at elevated temperatures and provides more active surface for ethanol oxidation (see Figure 2b, dotted line), as indirect effect.

From the Faradaic current plot (Figure 7a) we determine an apparent activation energy of $E_{app} = 32$ kJ/mol for ethanol oxidation over a Pt/Vulcan catalyst in the temperature range 30−60 °C (ethanol concentration 0.01 M, Pt loading 28 μg/cm^2, continuous mass transport, average charge for a full cycle). This value is, though bigger, of comparable magnitude as the 15−21 kJ/mol reported for methanol electrooxidation in the same temperature range.[19,28,30] On a first view the rather low value of the activation energy for ethanol oxidation is astonishing, because the (complete) oxidation of ethanol to CO_2 includes a C−C bond cleavage, which is expected to require higher activation energies.[5] It can be understood by the fact that the total rate is largely determined by the rates for incomplete

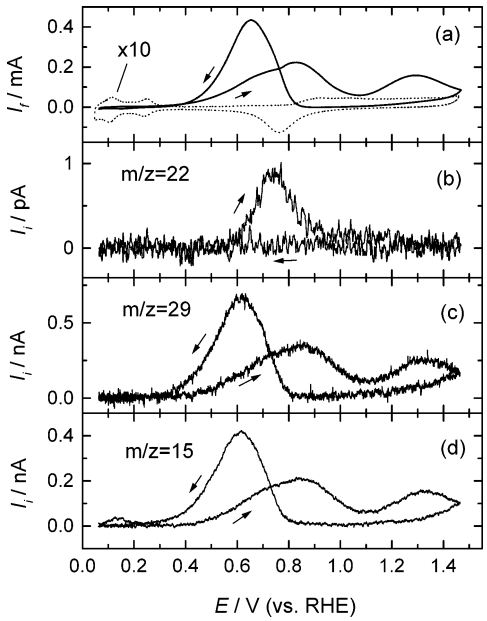

Figure 8. Simultaneously recorded CVs (a) and MSCVs for m/z = 22 (b), m/z = 29 (c), m/z = 15 (d), and m/z = 30 (e) for ethanol oxidation on a smooth polycrystalline Pt electrode in 0.1 M ethanol + 0.5 M H_2SO_4 solution. Scan rate: 10 mV/s, room temperature. Arrows indicate the direction of the potential scan. Dotted line (a) indicates the base CV of polycrystalline Pt in 0.5 M H_2SO_4 solution.

ethanol oxidation to acetic acid and acetaldehyde. Both byproducts still contain the C−C backbone and their formation requires only oxidation of the $-CH_2OH$ group. The barrier for this latter reaction should be not so different from that for methanol oxidation.

The apparent activation energy for ethanol oxidation to acetaldehyde, determined from Figure 7c, is 43 kJ/mol. Acetic acid formation (Figure 7d), which most likely occurs in a second step via further oxidation of acetaldehyde, rather than via direct oxidation of ethanol, has a lower apparent activation energy of 28 kJ/mol, although direct ethanol oxidation to acetic acid involves not only C−H bond splitting, but also oxygen addition to carbon and the formation of a new carbon−oxygen bond. Surprisingly, the apparent activation energy for CO_2 formation is only ca. 20 kJ/mol (Figure 7b), which can be understood by taking into account that in these potentiodynamic experiments CO_2 formation results mainly from the electrooxidation of the CO_{ad} species formed at lower potentials, as discussed above. This value agrees reasonably well with the activation barrier of 34 kJ/mol determined for CO electrooxidation on Pt(111) at 0.6 V in alkaline solution.[31]

3.4. Catalyst Loading Effect on Ethanol Electrooxidation Product Yields and Current Efficiency. In this section we will present the results of analogous DEMS experiments as shown in Figure 1 (section 3.1.1) performed on a smooth polycrystalline Pt electrode rather than on a supported Pt/Vulcan catalyst. We had shown in a previous study on the effects of catalyst loading on the reaction characteristics for methanol oxidation[26] that a smooth Pt electrode can be considered as a model system for a supported catalyst with a very low catalyst loading. That study revealed a considerable variation in reaction characteristics, product yields, and current efficiencies for methanol oxidation on supported Pt/Vulcan electrodes with decreasing catalyst loading, and finally a massive Pt electrode. Similar effects can be expected also for ethanol oxidation.

Figure 8 shows the dependence of the Faradaic current (a) and the corresponding m/z = 22 (b), m/z = 29 (c), and m/z = 15 (d) ion currents on the electrode potential during repetitive cycling for ethanol oxidation on a polycrystalline Pt electrode in 0.1 M C_2H_5OH containing solution and similar reaction conditions as in the EOR on Pt/Vulcan (see section 3.1.1 and Figure 1). The cyclic voltammogram (Figure 8a) resembles those reported in the literature[6−8,21] and the current−voltage characteristics for ethanol oxidation on Pt/Vulcan catalyst under the same conditions (Figure 1a), with the Faradaic current onset at about 0.4 V and the double peak with maxima at 0.73 and 0.85 V. It then passes through a second peak at 1.3 V in the positive-going scan, which agrees well with previous reports.[6−8,21] This peak is not observed in the EOR on Pt/Vulcan (see 3.1.1 and Figure 1a), because such positive potentials could not be applied due to oxidation of the carbon support.[22] The higher positive potential limit can also be the reason for the relatively higher anodic current peak in the negative-going scan for the polycrystalline Pt electrode (Figure 8a) compared to the Pt/Vulcan catalyst (Figure 1a). The ethanol oxidation current decreases to about 20% on the smooth polycrystalline Pt electrode (Figure 8a) compared to Pt/Vulcan (Figure 1a). It should be noted that the geometric area of the electrode exposed to the electrolyte is the same in both cases, which leads to the same diffusion-limited current for the purely mass transport-controlled process.

The general appearance of the mass spectrometric signals for CO_2 formation (Figure 8b) and acetaldehyde formation (Figure 8c,d) also resemble those observed for the Pt/Vulcan catalyst. The mass spectrometric current for acetaldehyde formation is only about one-fifth of the corresponding signals for the Pt/Vulcan catalyst (Figures 1c,d). Methane formation can be detected in the negative-going scan negative of 0.2 V (Figure 8d), whereas no ethane formation is found at these potentials (not shown here) on the smooth polycrystalline Pt electrode. It is important to note that both CO_2 and methane formation are more than 1 order of magnitude lower on the smooth polycrystalline Pt electrode than on the Pt/Vulcan catalyst (Figures 1b,d) for a similar difference in roughness factors (active surface areas) between the two electrodes (ca. 20 for Pt/Vulcan and 2 for polycrystalline Pt electrode, as determined from the H_{upd} charge). This also supports our previous conclusion that these species result mostly from surface reactions, namely either via oxidative stripping of CO_{ad} to CO_2, or via the reductive desorption of $CH_x(O)_{ad}$ hydrocarbon residues as methane,[12] rather than (purely) being limited by mass transport.

The current efficiency for CO_2 formation during ethanol oxidation on the polycrystalline Pt electrode, as before integrated over a complete potential scan cycle, is only ca. 1.2%, compared to 2.7% on the Pt/Vulcan catalyst at the same ethanol concentration (0.1 M). The current efficiencies for acetaldehyde and acetic acid are about 70% and 29%, respectively, compared to 35% and 62% on Pt/Vulcan. The corresponding product yields for CO_2, acetic acid, and acetaldehyde formation in ethanol oxidation reaction on polycrystalline Pt electrode are about 0.5%, 17%, and 82.5%, respectively, compared to ca. 1.5%, 45.5%, and 53% on Pt/Vulcan (see Table 1). This suggests that also for ethanol oxidation the roughness factor (or catalyst loading) of the electrode has a significant effect on the product distribution and the current efficiencies for CO_2, acetaldehyde, and acetic acid formation. Incomplete ethanol oxidation to acetaldehyde is favored on the smooth polycrystalline Pt electrode compared to the Pt/Vulcan catalyst.

These observations can be understood in a similar way as we had explained the variation of product yield with catalyst loading (or electrode roughness) for methanol oxidation on supported Pt/Vulcan catalyst electrodes with varying catalyst

loading.[26] In that case we had attributed the decreasing amount of volatile incomplete oxidation products, in particular of formaldehyde, to the increasing probability for readsorption, after desorption as (volatile) reaction intermediates, and the subsequent oxidation of the readsorbed species. This explanation was in good agreement also with the even lower amount of CO_2 formation on smooth Pt electrodes, where readsorption in a continuous flow of electrolyte is even less probable.[26,32,33] Following that reaction model one would expect preferable readsorption and further oxidation of volatile, oxidizable reaction intermediates (only acetaldehyde in the case of ethanol oxidation) on the Pt/Vulcan catalyst compared to a smooth polycrystalline Pt electrode. This model also explains the variation in product yields for ethanol oxidation upon varying the ethanol concentration (see section 3.2). As we had mentioned there, increasing ethanol concentration results in increasing coverages of a blocking adlayer, making readsorption less likely. Accordingly, one would expect less acetic acid formation and more acetaldehyde at higher ethanol concentrations, as was observed experimentally.

There is, however, a basic difference between methanol oxidation and ethanol oxidation. In contrast to the almost complete oxidation of methanol to CO_2 on a high loading Pt/Vulcan catalyst (28 $\mu g_{Pt}/cm^2$), the CO_2 yield for ethanol oxidation does not exceed a few percent, even on a comparable loading Pt/Vulcan catalyst (see Table 1). This basic difference between the two reactions is attributed to the very low rate for C−C bond breaking at relevant potentials, e.g., for continuous reaction at 0.61 V. For lower potentials dissociative adsorption of ethanol is possible but stops due to surface poisoning by decomposition products. CO_2 formation in cyclic voltammograms therefore reflects oxidation of adsorbed CO decomposition products. Furthermore, although both acetaldehyde and formaldehyde as volatile intermediates of the EOR and the MOR, respectively, can be further oxidized to the corresponding acids, acetic acid cannot be further oxidized to CO_2 at ambient temperatures.[25] In contrast, formic acid oxidation to CO_2 is facile under these conditions.[34] Considering these differences the effect of the catalyst loading or electrode roughness on the ethanol oxidation product yields agrees well with previous findings for the methanol oxidation reaction.

4. Conclusions

On the basis of a systematic study of the electrocatalytic ethanol oxidation on a carbon-supported Pt nanoparticle catalyst, including both cyclic voltammetry and potential step measurements of the reaction transients and using DEMS for the analysis and quantitative detection of the EOR product, we could quantitatively determine kinetic parameters (reaction orders, activation energies, steady-state rates) for the overall EOR and for the partial reactions leading to the individual reaction products CO_2, acetic acid, and acetaldehyde. From these results we can draw the following conclusions on the reaction process under present reaction conditions (continuous electrolyte flow, reaction temperature 23−60 °C, ethanol concentrations 1 mM to 0.5 M in 0.5 M sulfuric acid solution) on a well-defined Pt/Vulcan catalyst or on a smooth polycrystalline Pt electrode, respectively:

1. Incomplete ethanol oxidation to acetaldehyde and acetic acid prevails over complete oxidation to CO_2 under all conditions, the dominant products being acetic acid at low (1 mM) and acetaldehyde at high (0.5 M) ethanol concentration or low catalyst loading/roughness (on polycrystalline Pt). In a simple power law description of the rate we obtain an ethanol reaction order for the total reaction (Faradaic current) of 0.6 and ethanol reaction orders 0.3, 0.6, and 0.9 for the partial reactions leading to CO_2, acetic acid, and acetaldehyde, respectively.

2. Ethanol oxidation on a Pt/Vulcan catalyst is enhanced at elevated temperatures, the average overall apparent activation energy, integrated over a full potential cycle, being 32 kJ/mol for 0.01 M ethanol solution. The apparent activation energies for CO_2, acetic acid, and acetaldehyde formation, respectively, which are derived from the mass spectrometric signals, are 20, 28, and 43 kJ/mol. The current efficiency for complete oxidation to CO_2 decreases slightly with temperature due to the larger increase of acetaldehyde formation.

3. The comparable amounts of CO_2 formation (positive-going scan) and methane formation (negative-going scan) in the potentiodynamic oxidation experiments and in ethanol adsorbate stripping experiments suggest that these result from oxidation/reductive stripping of CO_{ad} and $CH_{x,ad}$ species formed at more negative potentials (CO_{ad} oxidation) or more positive potentials ($CH_{x,ad}$ oxidation), respectivley. This assignment is supported also by the rather low steady-state CO_2 formation current at 0.61 V, which is less than $^1/_{10}$th of the peak current for CO_2 formation during potentiodynamic CO_2 formation at the same potential. It explains also the rather low (1−10%) current efficiencies and product yields for CO_2 formation in the EOR.

4. The higher acetaldehyde (lower acetic acid) current efficiencies and product yields for ethanol oxidation on a smooth polycrystalline Pt electrode compared to a Pt/Vulcan catalyst on both surfaces can be explained in terms of increasing readsorption and further oxidation of volatile, *oxidizable* reaction intermediates, or byproducts (at ambient temperatures only acetaldehyde) on electrodes with increasing electrode roughness/catalyst loading. Because of the low probability for C−C bond breaking in the adsorbed C-2 molecules, and because acetic acid oxidation is inhibited at room temperature, the CO_2 yields are very low on both surfaces.

Finally, the data of the present study suggest that practical applications of ethanol-fed fuel cells with a carbon-supported Pt anode catalyst will demand operation at elevated temperatures because at ambient temperatures ethanol oxidation not only suffers from a low power density due to incomplete ethanol oxidation, but more importantly also from highly undesirable emissions of toxic byproducts (acetaldehyde). Higher operating temperatures and/or electrocatalysts being more efficient for C−C bond breaking are required to overcome these difficulties and to achieve complete oxidation of ethanol to CO_2.

Acknowledgment. We gratefully acknowledge financial support by the Deutsche Forschungsgemeinschaft (DFG) via grants Be 1201/8-4 and Be 1201/12-1, and by the Landesstiftung Baden-Württemberg via program "Portable Mini Fuel Cells".

References and Notes

(1) Wang, J.; Wasmus, S.; Savinell, R. F. *J. Electrochem. Soc.* **1995**, *142*, 4218.

(2) Schmidt, V. M.; Ianniello, R.; Pastor, E.; Gonzalez, S. *J. Phys. Chem.* **1996**, *100*, 17901.

(3) Fujiwara, N.; Friedrich, K. A.; Stimming, U. *J. Electroanal. Chem.* **1999**, *472*, 120.

(4) Lamy, C.; Belgsir, E. M.; Léger, J.-M. *J. Appl. Electrochem.* **2001**, *31*, 799.

(5) Nonaka, H.; Matsumura, Y. *J. Electroanal. Chem.* **2002**, *520*, 101.

(6) Bittins-Cattaneo, B.; Wilhelm, S.; Cattaneo, E.; Buschmann, H. W.; Vielstich, W. *Ber. Bunsen-Ges. Phys. Chem.* **1988**, *92*, 1210.

(7) Leung, L.-W. H.; Chang, S.-C.; Weaver, M. J. *J. Electroanal. Chem.* **1989**, *266*, 317.

(8) Hitmi, H.; Belgsir, E. M.; Leger, J. M.; Lamy, C.; Lezna, R. O. *Electrochim. Acta* **1994**, *39*, 407.

(9) Iwasita, T.; Pastor, E. *Electrochim. Acta* **1994**, *39*, 531.

(10) Schmiemann, U.; Müller, U.; Baltruschat, H. *Electrochim. Acta* **1994**, *40*, 99.
(11) Tarnowski, D. J.; Korzeniewski, C. *J. Phys. Chem. B* **1997**, *101*, 253.
(12) Wang, H.; Jusys, Z.; Behm, R. J. *Fuel Cells* **2004**, *4*, 113.
(13) Aricò, A. S.; Creti, P.; Antonucci, P. L.; Cho, J.; Kim, H.; Antonucci, V. *Electrochim. Acta* **1998**, *43*, 3719.
(14) Willsau, J.; Heitbaum, J. *J. Electroanal. Chem.* **1985**, *194*, 27.
(15) Ianniello, R.; Schmidt, V. M.; Rodriguez, J. L.; Pastor, E. *J. Electroanal. Chem.* **1999**, *471*, 167.
(16) Jusys, Z.; Behm, R. J. *J. Phys. Chem. B* **2001**, *105*, 10874.
(17) Schmidt, T. J.; Gasteiger, H. A.; Stäb, G. D.; Urban, P. M.; Kolb, D. M.; Behm, R. J. *J. Electrochem. Soc.* **1998**, *145*, 2354.
(18) Jusys, Z.; Massong, H.; Baltruschat, H. *J. Electrochem. Soc.* **1999**, *146*, 1093.
(19) Wakabayashi, N.; Uchida, H.; Watanabe, M. *Electrochem. Solid-State Lett.* **2002**, *5*, E62.
(20) Tremiliosi-Filho, G.; Gonzales, E. R.; Motheo, A. J.; Belgsir, E. M.; Leger, J. M.; Lamy, C. *J. Electroanal. Chem.* **1998**, *444*, 31.
(21) Iwasita, T.; Rasch, B.; Cattaneo, E. *Electrochim. Acta* **1989**, *34*, 1073.
(22) Roen, L. M.; Paik, C. H.; Jarvi, T. D. *Electrochem. Solid-State Lett.* **2004**, *7*, 19.
(23) Iwasita, T. *Brazil. J. Chem. Soc.* **2002**, *13*, 401.
(24) Leung, L. W. H.; Weaver, M. J. *J. Phys. Chem. B* **1988**, *92*, 4019.
(25) Wang, H.; Jusys, Z.; Behm, R. J. To be published.
(26) Jusys, Z.; Kaiser, J.; Behm, R. J. *Langmuir* **2003**, *19*, 6759.
(27) Wang, H.; Jusys, Z.; Behm, R. J. To be published.
(28) Madden, T. H.; Stuve, E. M. *J. Electrochem. Soc.* **2003**, *150*, E571.
(29) Kardash, D.; Korzeniewski, C. *Langmuir* **2000**, *16*, 8419.
(30) Schmidt, T. J.; Gasteiger, H. A.; Behm, R. *J. Electrochem. Commun.* **1999**, *1*, 1.
(31) Markovic, N. M.; Schmidt, T. J.; Grgur, B. N.; Gasteiger, H. A.; Behm, R. J.; Ross, P. N. *J. Phys. Chem. B* **1999**, *103*, 8568. *555*, 427.
(32) Wang, H.; Ch. Wingender, Baltruschat, H.; Lopez, M.; Reetz, M. T. *J. Electroanal. Chem.* **2001**, *509*, 163.
(33) Wang, H.; Löffler, T.; Baltruschat, H. *J. Appl. Electrochem.* **2001**, *30*, 759.
(34) Wolter, O.; Willsau, J.; Heitbaum, J. *J. Electrochem. Soc.* **1985**, *132*, 1635.